JOURNAL OF GUIDANCE, CONTROL, AND DYNAMICS
Vol. 32, No. 3, May–June 2009

Piecewise Global Volterra Nonlinear Modeling and Characterization for Aircraft Dynamics

Ashraf Omran* and Brett Newman†
Old Dominion University, Norfolk, Virginia 23529

DOI: 10.2514/1.40655

Evaluating global aircraft dynamic behavior by Volterra theory as an efficient nonlinear approximation method is investigated. In previous research, Volterra theory was implemented to evaluate the system behavior in a selected local region, which restricts the ability to capture the aircraft behavior while moving from one flight region to another. The current research presents a global piecewise Volterra kernel approach, which uses submodel Volterra kernels to build global kernels. A piecewise interpolation is employed to switch between the submodels. An approximate nonlinear pitch–plunge model for a high-performance aircraft was used to assess the proposed approach. A set of experimental simulations is conducted to verify the capability of the proposed model. The approach is compared with a global linear approach while employing the nonlinear simulation as the benchmark.

Nomenclature

A, B	=	impulse input amplitude
$C_{m\alpha}$	=	pitch moment coefficient with angle of attack, 1/ deg
$C_{m\delta e}$	=	pitch moment coefficient with elevator deflection, 1/ deg
C_Z	=	plunging force coefficient
f, g	=	generic function
h_k	=	Volterra kernel of kth order
q	=	pitch rate, deg /s
S	=	strength index
t, τ	=	time, s
t_H	=	horizon time, s
t_L, τ_L	=	time lag, s
u	=	input vector
u_o	=	operated input vector
x	=	state vector
y	=	output vector
α	=	angle of attack, deg
δ_e	=	elevator deflection, deg
δ_{eo}	=	operated elevator deflection, deg
θ	=	generic function
ϕ	=	generic function
ψ	=	generic function

I. Introduction

MATHEMATICAL modeling of aircraft dynamic behavior for analysis, understanding, and synthesis requires an efficient and accurate technique, especially when the aircraft moves from one flight regime to another. This process is compounded by system nonlinearities, including but not limited to aerodynamic derivatives, inertial coupling, and actuation limits, all leading to significant changes in dynamic characteristics across the flight envelope. Therefore, universal approaches to explore and evaluate dynamic behavior over all flight regimes are sought. One standard approach is based on nonlinear simulation with linear model extraction. The nonlinear simulation provides an accurate and specific solution for overall motion. However, these results are relatively more computation costly and less structured analytically. Linear analysis, on models generated at points along the overall motion, provides inexpensive relational solutions to local motion, which are relatively less precise but much broader. Unfortunately, this piecewise linearization technique for global analysis lacks the capability to capture nonlinear phenomena such as stalling, limit cycling, or inertial coupling. To overcome these analysis deficiencies, a nonlinear approximation method using a piecewise Volterra series is presented. This method is referred to as a global or universal Volterra method. The global model is represented as a set of kernels, where each kernel subset reflects the system characteristics in a specific region. In this way, extracting the Volterra kernels from the nonlinear simulation at various points can be a promising tool in describing and specifying the dynamic behavior of the aircraft over the entire flight domain.

Volterra theory has emerged as a popular nonlinear modeling technique, primarily because of the underlying analytical framework and its extension of the impulse response concept from linear theory. Volterra theory dates back to 1887, with the first encompassing publication appearing in 1927 and later 1958 [1,2]. An early use of this theory was made by Wiener and follow on research at the Massachusetts Institute of Technology in the area of filtering and electronic circuits [3–5]. The theory has received considerable attention in biomedical engineering as an efficient tool to identify nonlinear models of physiological systems experimentally [6], as well as in biologically inspired motion detection through vision processing [7]. In aeronautics, Volterra theory has been explored to a limited extent. Duffy [8] applies the approach to structural, fluid, and friction parameters affecting the stability of a compressor blade, in [9–11] the theory is used to identify the nonlinear aerodynamic response, in [12–15], to analyze the open- and closed-loop airfoil aeroelastic response, in [16], to identify nonlinear dynamics in aeroelastic/aeroservolastic lifting surfaces, and in [17], to study the F-18 active aeroelastic wing. A related topic is reduced-order modeling of unsteady fluid-structure systems using simplified model structures (Volterra kernels, for example) to match high-fidelity computational fluid-structure representations. Silva [18] provides a survey of current research in this area.

Few applications of the Volterra methodology to flight mechanics appear in the literature. Two notable exceptions are [19,20]. In these efforts, modeling the longitudinal dynamics of a high-performance aircraft in limit cycling conditions has been explored by the Volterra approach. In [20], a differential form of a reduced third-order Volterra series was considered. The approach proved the ability to capture the limit cycle, but the Volterra model still was restricted to a

Presented as Paper 6874 at the AIAA Atmospheric Flight Mechanics Conference and Exhibit, Honolulu, HI, 18–21 August 2008; received 31 August 2008; revision received 7 December 2008; accepted for publication 5 January 2009.

*Doctoral Student, Department of Aerospace Engineering. Student Member AIAA.

†Professor, Department of Aerospace Engineering. Associate Fellow AIAA.

certain equilibrium region. This work was extended in [19] to a global approach, which replaces the integral kernels with a repeatedly updated regression model using state-input memory values from the past three time steps and 24 regression coefficients. Although the approach showed satisfactory results, the approach is limited by only allowing system representation through finite sets of numerical coefficients and memory bits, thus destroying the underlying analytical function framework. Also an interesting application of Volterra theory in flight mechanics has been presented in [21] to define nonlinear flying quality metrics analytically. However, these efforts have been abandoned for more than 15 years because of computational difficulties in applying Volterra theory to strong nonlinearities in flight dynamic systems across the envelope. The current research aims to face these difficulties by proposing a piecewise global Volterra kernel approach. This approach breaks down the strong nonlinear model to a set of weak nonlinear submodels, and interpolation is then employed to move between the submodels. This reduction in computation simplifies the required mathematical manipulation to employ Volterra theory in flight mechanics.

This paper presents a global Volterra approach for characterizing the overall system dynamic behavior, which preserves the underlying functional framework in flight mechanics applications. Typically, the state of a dynamic system can be assigned to various domains inherent to the system, which could be linear and/or nonlinear. For example, attack angle and associated aerodynamic behavior is classified as prestall, stall, and poststall. These domains can reflect different stability tendencies. In prestall, the behavior is usually linear, but in the stall regime, the aerodynamics can be strongly nonlinear. In the poststall domain, the behavior can also be nonlinear but to a lesser extent. A set of Volterra series submodels can be generated for these various domains. An impulse response technique is used to estimate the Volterra kernels [22]. For computational efficiency, reduced-order Volterra terms are addressed. The order of the model is determined from a generic strength index metric. Subsequently, a piecewise Volterra kernel technique is used to switch between the Volterra submodels. The approach is applied to a simplified nonlinear model of a high-performance aircraft longitudinal dynamics [19]. Feasibility of the universal approach is determined by several input test cases. The test cases are compared with solutions generated from numerical integration of the nonlinear differential equations. Also, the proposed approach is compared with a global linear approach.

II. Volterra Theory

Many physical systems can be described across a set of nonlinear differential and algebraic equations between input, state, and output signals. A commonly used representation is the nonlinear state space form:

$$\dot{x}(t) = f\{t, x(t), u(t)\} \qquad y(t) = g\{t, x(t), u(t)\} \tag{1}$$

where $x \in R^n$ denotes the state vector, $u \in R^m$ the input vector, and $y \in R^p$ the output vector. Vectors $f \in R^n$ and $g \in R^p$ denote the system nonlinearities, and $t \in R^1$ is time. A few nonlinear systems are exactly solvable, many others, which are not tractable analytically, can be solved by numerical integration. Although numerical techniques can provide highly accurate results, analytical-type solutions are still sought. Their main advantage lies in their capability to interpret the physical meaning underneath a solution. The Volterra series is one such approach, which can represent a wide range of nonlinear system behavior. The theory represents the input–output relation of a nonlinear system as an infinite sum of multidimensional convolution integrals:

$$y(t) = h_o(t) + \sum_{k=1}^{\infty} \int_0^{\infty} \int_0^{\infty} \cdots \int_0^{\infty} h_k(\tau_1, \tau_2, \ldots, \tau_k) \cdot \prod_{i=1}^{k} u(t-\tau_i) \mathrm{d}\tau_i \tag{2}$$

In Eq. (2), $h_k(\tau_1, \tau_2, \ldots, \tau_k)$ denotes the kth-order Volterra kernel. The Volterra kernels are causal symmetric functions with respect to their argument [23].

To solidify the applicability of Eq. (2) and its origins, a conceptual derivation [2] is given first. The theory supposes that output $y(t)$ of a system at a particular time t depends nonlinearly on all values of the input at times equal and before t. In other words, $y(t)$ depends on $u(t-\tau)$ for all $\tau \geq 0$. If $u(t-\tau)$ can be quantified by the set $u_1(t), u_2(t), \ldots$, then output $y(t)$ is expressible as a nonlinear function of these quantities:

$$y(t) = \psi\{u_1(t), u_2(t), \ldots\} \tag{3}$$

The theory supposes the input $u(t-\tau)$ is given by an infinite series involving products of $u_i(t)$ with functions $\phi_i(\tau)$ serving as an orthonormal basis for the appropriate functional input vector space:

$$u(t-\tau) = \sum_{i=1}^{\infty} u_i(t)\phi_i(\tau) \tag{4}$$

$$\int_0^{\infty} \phi_i(\tau)\phi_j(\tau)\mathrm{d}\tau = \begin{cases} 1 & \text{for } i = j \\ 0 & \text{for } i \neq j \end{cases} \tag{5}$$

Exploiting the orthogonality property of $\phi_i(\tau)$, quantities $u_i(t)$ are computed as

$$u_i(t) = \int_0^{\infty} u(t-\tau)\phi_i(\tau)\mathrm{d}\tau \tag{6}$$

Finally expand Eq. (3) with a general power series, or

$$y(t) = \theta_0 + \sum_{i_1=1}^{\infty} \theta_{i_1} u_{i_1}(t) + \sum_{i_1=1}^{\infty}\sum_{i_2=1}^{\infty} \theta_{i_1 i_2} u_{i_1}(t) u_{i_2}(t) + \ldots \tag{7}$$

and substitute from Eq. (6) yielding

$$\begin{aligned} y(t) = \theta_0 &+ \int_0^{\infty} \sum_{i_1=1}^{\infty} \theta_{i_1}\phi_{i_1}(\tau_1)u(t-\tau_1)\mathrm{d}\tau_1 \\ &+ \int_0^{\infty}\int_0^{\infty} \sum_{i_1=1}^{\infty}\sum_{i_2=1}^{\infty} \theta_{i_1 i_2}\phi_{i_1}(\tau_1)\phi_{i_2}(\tau_2)u(t-\tau_1) \\ &\times u(t-\tau_2)\mathrm{d}\tau_1\mathrm{d}\tau_2 + \ldots \end{aligned} \tag{8}$$

Equation (8) has a term-by-term correspondence with Eq. (2) authenticating, for the purpose here, the Volterra series solution. A more rigorous mathematical proof can be found in [1,2].

In general kernels are of two classes: the state-dependent class and the input-dependent class. The only member of the state-dependent class is kernel $h_o(t)$, which represents the response of the output due to the initial system state, but which also depends indirectly on the input. If the system motion is started at an equilibrium condition (both state and input values) and the equilibrium input is maintained, kernel $h_o(t)$ equals zero. On the other hand, if the state value is mismatched to the equilibrium input, or vice versa, kernel $h_o(t)$ is nonzero and can be interpreted as motion of the system from the initial state to the equilibrium state (stable), or the state reacting to the input. Sometimes the $h_o(t)$ response can be a sustained oscillation representing a limit cycle, or possess a divergent behavior for an unstable equilibrium. The input-dependent class contains all other Volterra kernels. Those kernels represent the behavior of the system to any arbitrary input. In this class, each Volterra kernel is represented with the input in a multidimensional convolution integration. Each kernel appearing in the convolution integrals reflects a specific system behavior. Both the state- and input-dependent class kernels are unique for a given system. For weak nonlinearities, all higher-order kernels are seen to quickly tend to negligible values in the system representation. For a completely linear system, only $h_o(t)$ and $h_1(t)$ remain.

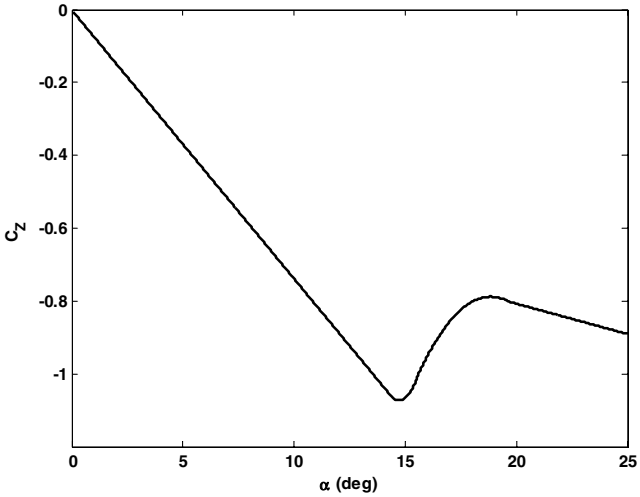

Fig. 1 Nonlinear plunging force coefficient $C_z(\alpha)$.

III. Kernel Identification

Kernels are the backbone of Volterra theory, but these kernels must be constructed by some means. Several methodologies have been addressed in the literature to estimate the Volterra kernels. Some methods are analytical in nature, consisting of an integral form [7] or differential form [19]. Other proposed methods are numerical procedures to identify the nonlinear system treated as a black box or gray box. Some techniques are based on linear regression or least square estimation (LSE). LSE can be cast as a recursive algorithm [6,20,24] or a nonrecursive algorithm [25–27]. Another method to estimate Volterra kernels from the system identification point of view is provided by the use of sinusoidal or impulsive inputs [9,23]. The strategy is an extension from the use of impulsive and sinusoidal inputs to identify linear systems. This strategy captures only the input–output behavior of a system and disregards any internal structure.

In this research, Volterra kernel estimation via impulsive input is implemented. The kernels are estimated from a time domain system identification perspective. As the input $u(t)$ is applied to and the output $y(t)$ is recorded from the undefined system, the waveform of the output and input signals are used to estimate the kernels. This methodology is especially favorable for reflecting the operational meaning of Volterra kernels. For an impulsive input, every kernel indicates the response of the system as a function of time and a certain number of distinct time lags. For example, a second-order kernel is a function of both time and time lag τ_L, or $h_2(t, t-\tau_L)$, which reflects how the system memory (nonlinearity) from an applied input at previous time $(t-\tau_L)$ affects the response of the system with input at time t. Based on the operational meaning of the kernel and the input time lag, kernel identification can be realized by inputting a signal waveform of multiple impulses with variable amplitude and variable time lag.

A procedure is given in [23] for first- and second-order kernel estimation, which is generalized here to nth order. The diagonal values of n kernels are estimated by applying a sequence of variable strength impulse inputs one at a time as

$$u_i(t) = A_i\delta(t), \qquad i = 0, 1, 2, \ldots, n \tag{9}$$

Each input generates a corresponding response $y_i(t)$ as

$$y_i(t) = h_o(t) + A_i h_1(t) + A_i^2 h_2(t,t) + \cdots + A_i^n h_n(t,t,\ldots,t) \qquad i = 0, 1, 2, \ldots, n \tag{10}$$

Equation (10) represents a set of simultaneous equations for the diagonal kernel values. These diagonal values are computed as

$$\begin{aligned} &h(t) = A^{-1}y(t) \\ &h(t) = [\,h_0(t) \quad h_1(t) \quad h_2(t,t) \quad \cdots \quad h_n(t,t,\ldots,t)\,]^T \\ &y(t) = [\,y_0(t) \quad y_1(t) \quad \ldots \quad y_n(t)\,]^T \\ &A = \begin{bmatrix} 1 & A_0 & A_0^2 & \ldots & A_0^n \\ 1 & A_1 & A_1^2 & \ldots & A_1^n \\ \vdots & & & & \vdots \\ 1 & A_n & A_n^2 & \ldots & A_n^n \end{bmatrix} \end{aligned} \tag{11}$$

This computation is carried out at each point in the time series. The impulse strengths must be selected to ensure excitation of relevant nonlinearities and invertibility of the $(n+1)\times(n+1)$ matrix A.

This methodology can be extended to estimate off-diagonal values of the high-order kernels by exciting the system through a sequence of time-delayed impulses. The m off-diagonal kernel values are estimated by applying a sequence of variable strength time-delayed impulse inputs one at a time.

$$u_i(t) = A_i\delta(t) + B_i\delta(t-t_L), \qquad i = 1, 2, \ldots, m \tag{12}$$

The produced responses corresponding to these inputs are

$$\begin{aligned} y_i(t) = {} & h_o(t) + A_i h_1(t) + B_i h_1(t-t_L) + A_i^2 h_2(t,t) \\ & + 2A_iB_i h_2(t,t-t_L) + B_i^2 h_2(t-t_L,t-t_L) + \cdots \\ & + A_i^n h_n(t,t,\ldots,t) + \frac{n}{1}A_i^{n-1}B_i h_n(t,\ldots,t,t-t_L) \\ & + \frac{n(n-1)}{1\cdot 2}A_i^{n-2}B_i^2 h_n(t,\ldots,t,t-t_L,t-t_L) + \cdots \\ & + \frac{n(n-1)}{1\cdot 2}A_i^2B_i^{n-2} h_n(t,t,t-t_L,\ldots,t-t_L) \\ & + \frac{n}{1}A_iB_i^{n-1} h_n(t,t-t_L,\ldots,t-t_L) \\ & + B_i^n h_n(t-t_L,t-t_L,\ldots,t-t_L) \quad i = 1,2,\ldots,m, \quad m = \sum_{i=1}^{n-1} i \end{aligned} \tag{13}$$

Equation (13) also represents a set of simultaneous equations, this time for the off-diagonal kernel values. These off-diagonal values are computed as

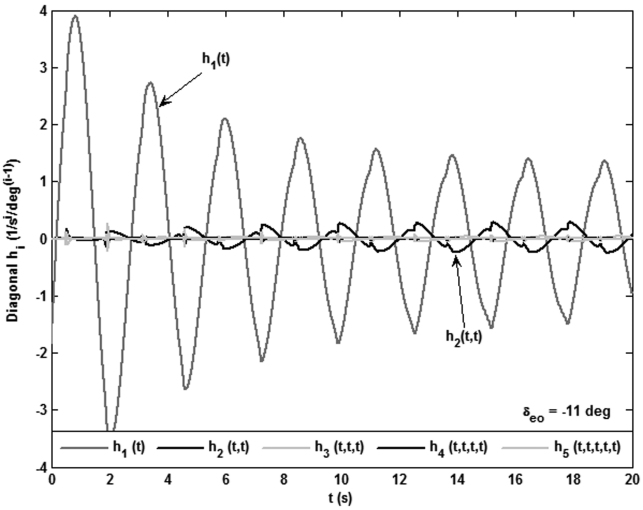

Fig. 2 Diagonal kernel responses of fifth-order model in stall/poststall subspace.

$$h'(t) = [AB]^{-1} y'(t) \qquad h'(t) = \begin{bmatrix} h_2(t, t-t_L) \\ h_3(t,t,t-t_L) \\ h_3(t,t-t_L,t-t_L) \\ \vdots \\ h_n(t,\ldots,t,t-t_L) \\ h_n(t,\ldots,t,t-t_L,t-t_L) \\ \vdots \\ h_n(t,t,t-t_L,\ldots,t-t_L) \\ h_n(t,t-t_L,\ldots,t-t_L) \end{bmatrix}$$

$$y'(t) = \begin{bmatrix} y_1(t) - h_0(t) - A_1 h_1(t) - B_1 h_1(t-t_L) - A_1^2 h_2(t,t) - B_1^2 h_2(t-t_L,t-t_L) - \cdots - A_1^n h_n(t,t,\ldots,t) - B_1^n h_n(t-t_L,t-t_L,\ldots,t-t_L) \\ y_2(t) - h_0(t) - A_2 h_1(t) - B_2 h_1(t-t_L) - A_2^2 h_2(t,t) - B_2^2 h_2(t-t_L,t-t_L) - \cdots - A_2^n h_n(t,t,\ldots,t) - B_2^n h_n(t-t_L,t-t_L,\ldots,t-t_L) \\ \vdots \\ \vdots \\ \vdots \\ y_m(t) - h_0(t) - A_m h_1(t) - B_m h_1(t-t_L) - A_m^2 h_2(t,t) - B_m^2 h_2(t-t_L,t-t_L) - \cdots - A_m^n h_n(t,t,\ldots,t) - B_m^n h_n(t-t_L,t-t_L,\ldots,t-t_L) \end{bmatrix}$$

$$[AB] = \begin{bmatrix} 2A_1B_1 & 3A_1^2B_1 & 3A_1B_1^2 & \cdots & \frac{n}{1}A_1^{n-1}B_1 & \frac{n(n-1)}{1\cdot 2}A_1^{n-2}B_1^2 & \cdots & \frac{n(n-1)}{1\cdot 2}A_1^2B_1^{n-2} & \frac{n}{1}A_1B_1^{n-1} \\ 2A_2B_2 & 3A_2^2B_2 & 3A_2B_2^2 & \cdots & \frac{n}{1}A_2^{n-1}B_2 & \frac{n(n-1)}{1\cdot 2}A_2^{n-2}B_2^2 & \cdots & \frac{n(n-1)}{1\cdot 2}A_2^2B_2^{n-2} & \frac{n}{1}A_2B_2^{n-1} \\ \vdots & & & & & & & & \\ \vdots & & & & & & & & \\ 2A_mB_m & 3A_m^2B_m & 3A_mB_m^2 & \cdots & \frac{n}{1}A_m^{n-1}B_m & \frac{n(n-1)}{1\cdot 2}A_m^{n-2}B_m^2 & \cdots & \frac{n(n-1)}{1\cdot 2}A_m^2B_m^{n-2} & \frac{n}{1}A_mB_m^{n-1} \end{bmatrix} \tag{14}$$

This computation is carried out at each point in the time series. The impulse strengths are selected to strongly excite the nonlinearities of interest and to avoid singularity of the $m \times$ m matrix $[AB]$. By varying the value of t_L from zero to t_H, the desired temporal horizon of the Volterra model, the value of any kernel at an off-diagonal point in the domain can be defined numerically. It is only necessary to calculate the kernels over half of the domain with this procedure, the remaining half is obtained from kernel symmetry. If only two kernels through $h_2(t, t-t_L)$ are sought, the preceding general technique simplifies considerably. Equation (13) reduces to a single equation and the matrix inverse solution in Eq. (14) is replaced by scalar division

$$\begin{aligned} y(t) &= h_o(t) + Ah_1(t) + Bh_1(t-t_L) + A^2h_2(t,t) \\ &\quad + 2ABh_2(t,t-t_L) + B^2h_2(t-t_L,t-t_L) \\ h_2(t,t-t_L) &= \frac{1}{2AB}\{y(t) - h_o(t) - Ah_1(t) - Bh_1(t-t_L) \\ &\quad - A^2h_2(t,t) - B^2h_2(t-t_L,t-t_L)\} \end{aligned} \tag{15}$$

The traditional technique to determine the number of required terms for modeling the system dynamics is based on trial and error. First, a model with n terms is initially constructed. The model is then compared with the nonlinear simulation for some test cases. New terms are included, or existing terms are deleted, depending on the comparison results. The technique is a trade-off between number of terms and response accuracy. This technique is time consuming, and the simulated test cases cannot cover all possibilities of system behavior. For these reasons, a new function called the "strength index" S is proposed in the current research. This index uses the estimated diagonal values of each input-dependent kernel, instead of the extensive simulation across all kernels, to judge their importance. The index S_i is defined as a convolution line integral over the diagonal kernel of ith order multiplied by the same order of input, as demonstrated in Eq. (16). An absolute value applied to the integral argument will be preferred to avoid the possibility of integral area cancelling. Each index S_i is considered as a gauge to measure the magnitude of each term in the system model. Thus, a large strength index value for S_i, relative to S_1, means that the corresponding kernel has a significant contribution in rendering the system behavior, and vice versa. In this way, Eq. (16) is used to determine how many terms should be considered in the model. An underlying assumption in the strength index definition that is diagonal kernel values are larger than or equal to the off-diagonal values. Although not guaranteed, this characteristic is typically maintained when the expansion point is asymptotically or neutrally stable and the casual symmetric kernel functions decay or oscillate with the temporal arguments. As an example, kernels displayed in [12,13,23] behave in this manner:

$$S_i = \int_0^{t_H} |h_i(\tau,\tau,\ldots,\tau)u(\tau)^i| \mathrm{d}\tau \qquad \text{where } i = 1, 2, 3, \ldots, n \tag{16}$$

IV. Global Kernel Methodology

The number of Volterra series terms required to model the system behavior depends on two main attributes. The first one is the operating space range to be covered by the model. Hence, the series is expanded around an operating point, and a wider range to be captured by the model requires more terms in the series. Unfortunately, the convolution integral becomes ever more computationally expensive with more terms. For example, suppose a fifth-order Volterra series is required in a certain model over a certain range. The model will involve a potentially prohibitive fifth-dimensional integral. Further, suppose the range consists of two subranges where the model can be replaced by two submodels of second- or third-order Volterra series. The new model will require less computation. The second attribute is

that the strength of the nonlinearity involved in the system reflects the number of required Volterra series terms in the sense of more terms for more nonlinearity. Suppose for example a sharp change nonlinearity like saturation requires a fifth-dimensional integral. If the true nonlinearity is simplified by a smooth saturation, the new model may only require a second- or third-order Volterra series model. Another example is given in [20], when the sharp change in the plunge force coefficient with angle of attack was simplified by a smooth variation. In this way, a third-order Volterra series was sufficient. These attributes show that sometimes the overall behavior of the system cannot, or should not, be represented by a single series high-order expansion. This paper focuses on the range attribute.

An important issue concerns the switching between submodel Volterra series, when the system transitions from one operating point to another across several subranges. Global linear models are typically constructed based on the interpolation between the linear submodels at different operating points. A linear-gain scheduled control system is a prime example. In this way, use of a global Volterra series is proposed. This approach is addressed by employing the submodel Volterra kernels in an interpolation procedure. Effectively a new dimension is added to the series kernels. For example, the first kernel will have two arguments instead of one, or $h_1(t, u_o)$ instead of $h_1(t)$, where u_o is the operating point around which the submodel is constructed. An interpolation technique is used to move through the tables of Volterra kernels. The number of submodels and the range of each model may have a large effect on global model accuracy, therefore an intelligent sequence is outlined here to find an appropriate number of the submodels and the range of each one. The sequence is organized as shown next.

1) Select an operating point within a candidate subspace. The selected operating points should lay in a region of stability. In this way, all the estimated kernels either diminish or oscillate as the time arguments $(\tau_1, \tau_2, \ldots)$ grow to infinity.

2) Assume an nth-order Volterra series model as an initial trial.

3) Use Eq. (11) to compute the state-dependent kernel and the diagonal value of each input-dependent kernel. Compute the strength index of each input-dependent kernel using Eq. (16).

4) Compare the strength index value of each kernel with respect to the first kernel. If the strength ratio is more than a specific tolerance, then the kernel is considered to be significant in the model.

5) Reduce or expand the order of the model based on the strength ratio results.

6) Render the subspace by exciting the approximate model by a step input with different amplitudes and compare the response to the nonlinear simulation. The subspace is defined as the region where the response error is within a specified tolerance.

7) Sweep the operating point forward and backward across the subspace and return to step 2 to maximize the range and minimize the number of kernels.

Because convergence of the Volterra series generation is excitation amplitude dependent, these amplitudes must be carefully chosen. Amplitude selection is based on constraining the responses to remain within the subregion of interest while simultaneously forcing the responses to transit nearly all of the subregion. Selecting amplitude in this way allows for identification of nonlinearities residing within the subregion of interest and avoids convergence issues associated with computing higher-order kernels across all subregions with large amplitude excitation. Because accuracy of the Volterra series is strength index cutoff dependent, the cutoff must be chosen for the intended application. For the application of system analysis, rather than high-fidelity simulation, a cutoff of 10% is reasonable. If a kernel is contributing less that 10% relative to the base kernel, then the model derived by neglecting that kernel is expected to be 90% accurate. This level of accuracy is sufficient for analysis purposes. If the kernels are computed from data containing measurement noise, which is not the case here, the cutoff could be raised to filter out kernels with increased amplitudes due to noise transients.

V. Longitudinal Aircraft Model

A simplified longitudinal dynamic model of a high-performance aircraft is chosen as an example for the proposed approach. The model is addressed in [19,20] for the short-period mode, where the motion involves rapid changes to the angle of attack and pitch attitude at roughly constant airspeed. The suitability of this model is that the dynamics cover both linear and nonlinear flight behavior through an extensive range in angle of attack. The model is mathematically described as [20]

$$\dot{\alpha} = q + 9.168C_Z(\alpha) - 1.834(\delta_e + 7\,\text{deg}) + 7.362 \qquad \dot{q} = 5.730(C_{m\alpha}\alpha + C_{m\delta e}\delta_e) + 2.865$$

$$\text{where } C_Z(\alpha) = \begin{cases} -0.07378\alpha, \alpha \le 14.36\,\text{deg} & \text{(prestall)} \\ 0.09722\alpha^2 - 2.865\alpha + 20.04, 14.36\,\text{deg} \le \alpha \le 15.6\,\text{deg} & \text{(prestall/stall)} \\ -0.01971\alpha^2 + 0.7439\alpha - 7.808, 15.6\,\text{deg} \le \alpha \le 19.6\,\text{deg} & \text{(stall/poststall)} \\ -0.4733 - 0.01667\alpha, 19.6\,\text{deg} \le \alpha & \text{(poststall)} \end{cases} \tag{17}$$

In Eq. (17), α is the angle of attack in degrees, q is the pitch rate in degrees per second, δ_e is the elevator control surface deflection in degrees, $C_Z(\alpha)$ is the plunging force coefficient, $C_{m\delta e}$ is the pitch moment coefficient with elevator deflection, and $C_{m\alpha}$ is the pitch moment coefficient with angle of attack. The model is simplified further by fixing the pitching coefficients as $C_{m\alpha} = -1\text{deg}^{-1}$ and $C_{m\delta e} = -1.5\text{deg}^{-1}$. The sole nonlinearity in the model is the plunging force coefficient $C_Z(\alpha)$. The coefficient behavior is shown in Fig. 1. The nonlinearity approximates stall and lift recovery at high attack angles. The $C_Z(\alpha)$ model originally was discrete data points collected from a wind tunnel test. The coefficients in Eq. (17) were then numerically computed to provide a fit for these points over the corresponding α intervals as mentioned in [19,20].

Figure 1 shows how the plunging force coefficient has different values of slope. Every distinct slope demonstrates different characteristics in system behavior. The constant slope value in the prestall and poststall regions renders linear system behavior. From the linear perspective, the system is plunge axis statically stable in

Table 1 Kernel strength indices

Subspace index	Range, deg	δ_{eo}, deg	S_1, deg	S_2, deg	S_3, deg	S_4, deg	S_5, deg
1	$\alpha \le 14.36$	0	7.732	2.3×10^{-12}	2.0×10^{-12}	9.9×10^{-12}	1.7×10^{-12}
2	$14.36 \le \alpha \le 15.6$	−9.5	23.705	2.3001	0.5676	0.2201	0.0823
3	$15.6 \le \alpha \le 19.6$	−11	24.602	2.2332	0.4541	0.1501	0.0548
4	$19.6 \le \alpha$	−14	25.052	1.8005	0.2737	0.0766	0.0272

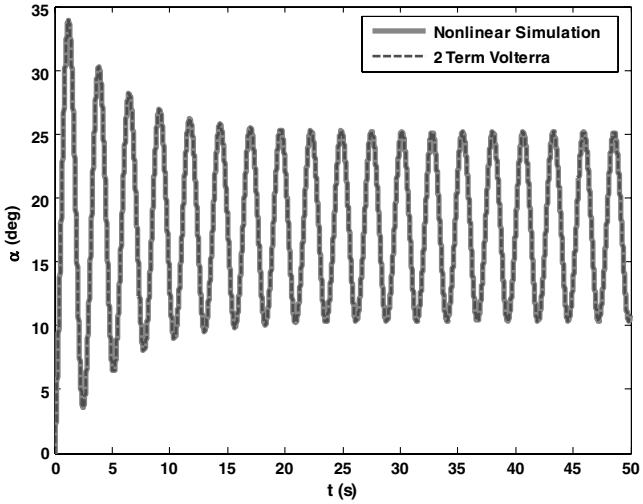

Fig. 3 Angle-of-attack step response of stall/poststall submodel.

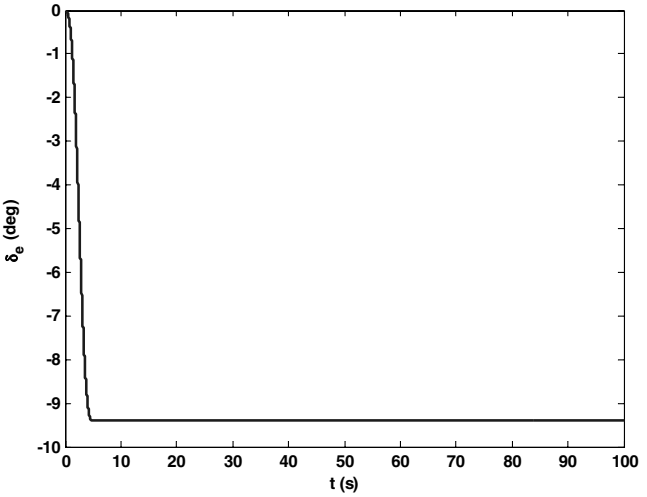

Fig. 4 Step input test case.

these regions. Thus, a negative rate of change in plunging force coefficient creates a damping plunge force counteracting the original perturbation. Along with the negative pitch axis static stability ($C_{m\alpha} < 0$), this damping force contributes to the aircraft returning to trimmed equilibrium flight in the sense of dynamic stability. Note in the prestall regime, the settling time is less than in the poststall regime, because of the larger slope value in Fig. 1. On the other hand, the significant curvature in the stall regime renders nonlinear system behavior. The stall regime can be split into two subregimes. The first is the prestall/stall regime. In this subregime, the slope switches from negative to positive or from stability to instability. The second is the stall/poststall regime, where the slope switches from instability to stability. Both subregimes capture the nonlinear behavior of the system as a limit cycle phenomenon. Note the classical pitch static margin characterization of stability is not applicable to the Eq. (17) model having a fixed $C_{m\alpha}$ but independently varying nonlinear $C_Z(\alpha)$. Also note the nonlinearity is a function of the angle of attack, but elevator deflection is the core mechanism to move through the various regimes. For the case of stable linear behavior, the analogous value of elevator deflection is below -9.5 deg or above -11 deg, and in between these values limit cycle behavior is experienced.

VI. Example Results

An example addressing the construction, validation, and use of a global aircraft dynamic model using piecewise Volterra kernels based on the aircraft model in Sec. V and the submodel construction process in Sec. IV is offered. Subspace modeling was previously addressed in [19,20]. Modeling there was based on dividing the operating space into a finite number of subspaces employing different operating points and different series orders. Here the space is divided into four subspaces based on the range of elevator deflection, consistent with Eq. (17). Two subspaces exist for linear behavior in the prestall and the poststall regions, and two for nonlinear behavior in the stall regimes also exist. For the two nonlinear subspaces, the points around which the series were expanded were selected to have a negative slope. For example, in the prestall/stall subspace, C_Z initially decreases with increasing angle of attack (negative slope) until a minimum point ($\alpha = 14.74$ deg or $\delta_{eo} = -9.5$ deg) is reached. After this minimum point, C_Z increases with an increasing angle of attack (positive slope). To avoid expanding on unstable behavior (positive slope), the operating point is selected to be $\delta_{eo} = -9.5$ deg. In the same way, the operating point is selected in the stall/poststall subspace. This careful selection is a critical feature for success but it places the expansion points near the edge of the subregions.

Table 2 Differential Volterra parameters of Eq. (18)

Subspace index	A_{11}, 1/s	δ_{eo}, deg	$g(\alpha_1)$, deg/s
1	−0.668	0	0
2	−0.671	−9.5	$0.891\alpha_1^2$
3	0.459	−11	$-0.181\alpha_1^2$
4	−0.153	−14	0

After selecting the operating points, a fifth-order Volterra series model is initially assumed as mentioned in Sec. IV. The diagonal waveforms of the kernels are computed for an angle of attack output signal, expanded around $\alpha = 0$ deg and the elevator operating point value δ_{eo}, as a set of simultaneous equations as in Eq. (11). One test case of the diagonal kernels is presented in Fig. 2 for the stall/poststall subspace. These diagonal kernel waveforms are estimated around an operating point defined by $\delta_{eo} = -11$ deg. Note the operating point can be defined by elevator deflection or the corresponding angle of attack at trim. Figure 2 shows that the first kernel is the most significant followed by the second diagonal kernel. This qualitative observation can help in deciding how to reduce the order of the submodel, but it is preferable to base this judgment on quantitative numerical criteria such as the strength index.

A strength index is used to evaluate the number of terms required to render the system's behavior in each subspace. Table 1 mentions the value of the strength indices in each subspace. Each index is computed by numerical integration. A 20 s time span and a unit step input are considered. Several iterations are conducted searching for optimal operating points and ranges (see Table 1) based on the sequence listed in Sec. IV. The ratios between the strength of the first

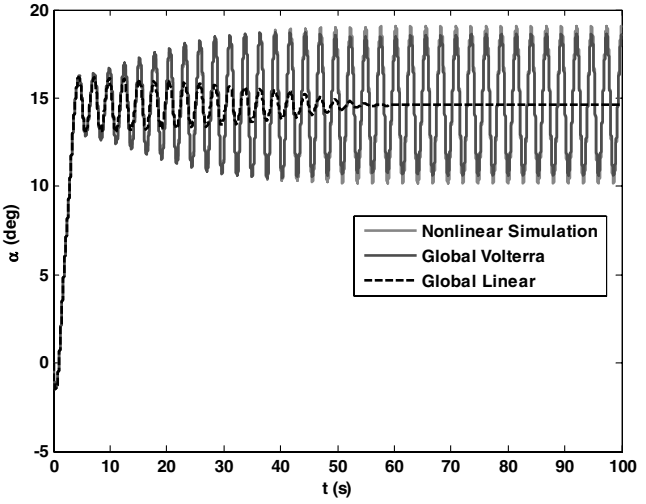

Fig. 5 Step response test case.

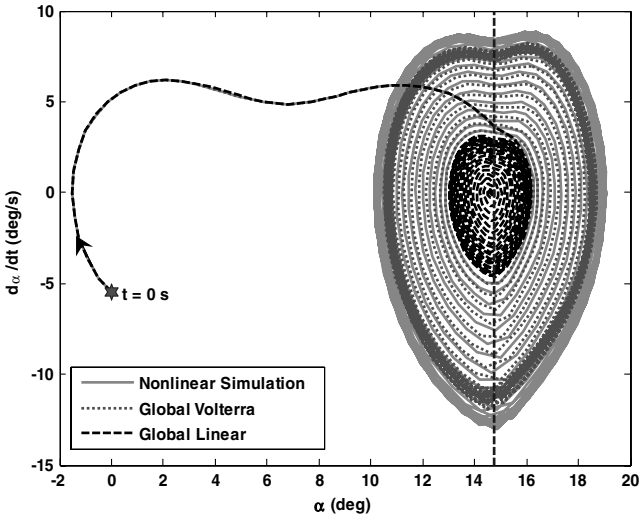

Fig. 6 Phase plane of step response test case.

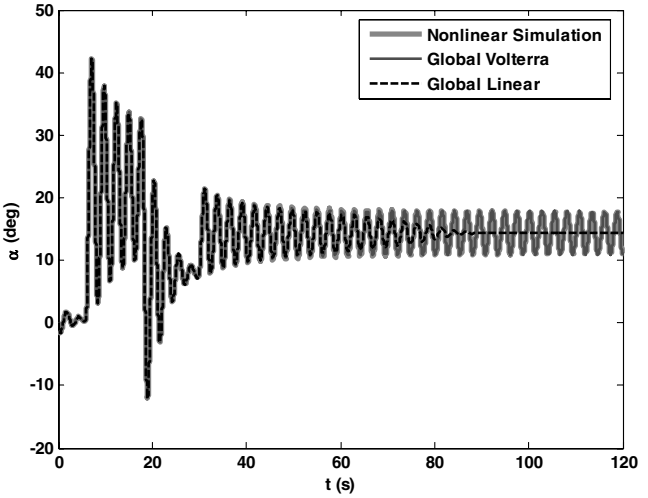

Fig. 8 Bang-bang response test case.

kernel S_1 and higher-order strengths change from one subspace to another depending on the level of nonlinearity. In the first subspace, the strength index of the first kernel is the only significant value compared with the others. The strength index of the second kernel S_2 is raised in the second subspace to be approximately 10% of the strength index of the first kernel. This quantification means the nonlinearity starts to appear in a significant way. The ratio of S_2 to S_1 in the second subspace is the same as in the third subspace implying the level of nonlinearity in the second and third subspaces is the same. In the fourth subspace, the ratio S_2/S_1 decreases to 7% indicating reduced but still significant nonlinearity. The strength indices of the third- and higher-order kernels have very small values with less than 2% strength of S_1 in all subspaces. All these results indicate that the first- and second-order kernels are sufficient to render the system angle-of-attack behavior in all subspaces. The off-diagonal second-order kernel values are then constructed. This overall kernel generation procedure was implemented on a desktop computer with sufficient turn around time.

The accuracy of each submodel is evaluated by step input excitation. A step input is used with different amplitudes. The estimated response is compared with the result of the nonlinear simulation. Figure 3 shows a comparison between the stall/poststall Volterra series second-order model and the nonlinear simulation response to a step input of -0.5 deg from the initial operating values $\delta_{eo} = -11$ deg and $\alpha = 0$ deg. The second-order submodel is sufficiently accurate, even as the angle of attack crosses all four regions. However an increase in the amplitude of the input leads to a decrease in the accuracy. The results show how the reduced second-order submodel of the Volterra series are able to render the system behavior in the respective subspaces.

Combining the four submodels into a global model and assessing the accuracy across the entire operating range is addressed next. For numerical simulation, a differential equation form of the Volterra series is more convenient than the integral form [20]. This differential form is based on breaking the original nonlinear differential equations into a sequence of pseudolinear time invariant systems where the input to the next system is a nonlinear function of the previous system output. This model structure consisting of a static nonlinear mapping function cascaded with an linear time invariant system is in the form of a Hammerstein model [28]. Although commonly assumed as a model structure in other disciplines [29], the Hammerstein structure here naturally results from the Volterra integral to the Volterra differential conversion process. Based on Table 1, two terms of a Volterra series are enough to capture the system behavior for all regions using this piecewise interpolation technique. Thus, Eq. (17) is broken down as the two pseudolinear differential equation sets

$$\begin{bmatrix} \dot{\alpha}_1 \\ \dot{q}_1 \end{bmatrix} = \begin{bmatrix} A_{11} & 1 \\ -5.73 & 0 \end{bmatrix} \begin{bmatrix} \alpha_1 \\ q_1 \end{bmatrix} + \begin{bmatrix} -1.834 \\ 8.595 \end{bmatrix} (\delta_e - \delta_{eo}) \tag{18a}$$

$$\begin{bmatrix} \dot{\alpha}_2 \\ \dot{q}_2 \end{bmatrix} = \begin{bmatrix} A_{11} & 1 \\ -5.73 & 0 \end{bmatrix} \begin{bmatrix} \alpha_2 \\ q_2 \end{bmatrix} + \begin{bmatrix} g(\alpha_1) \\ 0 \end{bmatrix} \tag{18b}$$

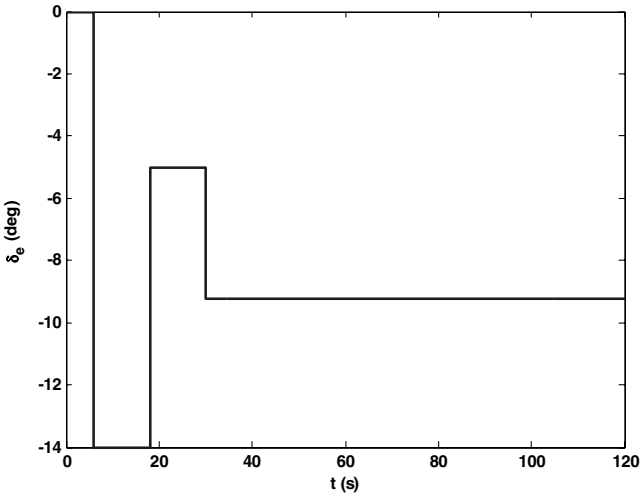

Fig. 7 Bang-bang input test case.

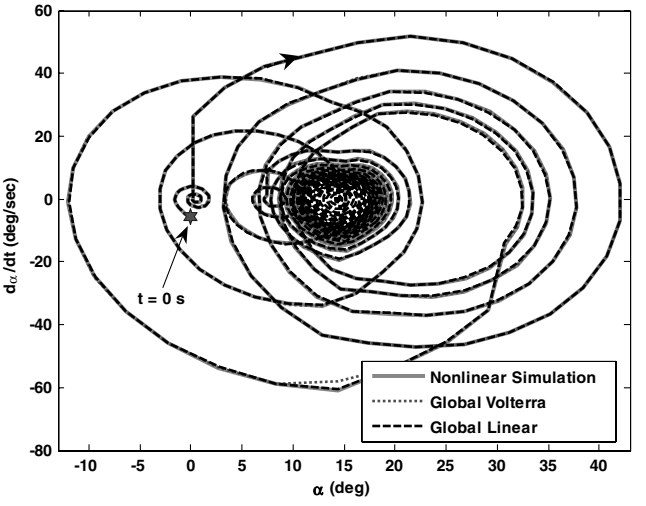

Fig. 9 Phase plane of bang-bang response test case.

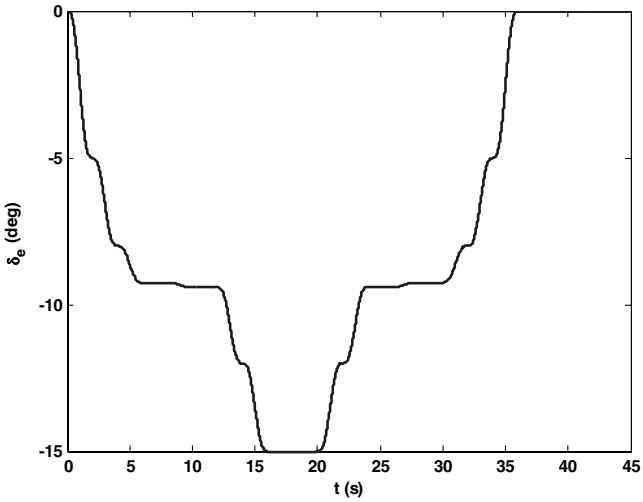

Fig. 10 Stair input test case.

where A_{11}, δ_{eo}, and $g(\alpha_1)$ have different values for each subspace as given in Table 2, and the output α equals the summation of states α_1 and α_2. Along with nonlinear simulation, the global Volterra approach is also compared with a linear global approach. The model is previously derived in [20] for local behavior evaluation. The model is a piecewise linear model of $C_z(\alpha)$. The state space model is documented in Eq. (19)

$$\begin{bmatrix}\dot{\alpha}\\ \dot{q}\end{bmatrix}=\begin{bmatrix}-0.668 & 1\\ -5.73 & 0\end{bmatrix}\begin{bmatrix}\alpha\\ q\end{bmatrix}+\begin{bmatrix}-1.834\\ 8.595\end{bmatrix}\delta_e+\begin{bmatrix}12.84\\ 2.865\end{bmatrix}$$
$$\alpha \le 14.74\ \text{deg} \tag{19a}$$

$$\begin{bmatrix}\dot{\alpha}\\ \dot{q}\end{bmatrix}=\begin{bmatrix}0.811 & 1\\ -5.73 & 0\end{bmatrix}\begin{bmatrix}\alpha\\ q\end{bmatrix}+\begin{bmatrix}-1.834\\ 8.595\end{bmatrix}\delta_e+\begin{bmatrix}-34.60\\ 2.865\end{bmatrix}$$
$$14.74\ \text{deg} < \alpha \le 17.4\ \text{deg} \tag{19b}$$

$$\begin{bmatrix}\dot{\alpha}\\ \dot{q}\end{bmatrix}=\begin{bmatrix}0.312 & 1\\ -5.73 & 0\end{bmatrix}\begin{bmatrix}\alpha\\ q\end{bmatrix}+\begin{bmatrix}-1.834\\ 8.595\end{bmatrix}\delta_e+\begin{bmatrix}-25.73\\ 2.865\end{bmatrix}$$
$$17.4\ \text{deg} < \alpha \le 18.87\ \text{deg} \tag{19c}$$

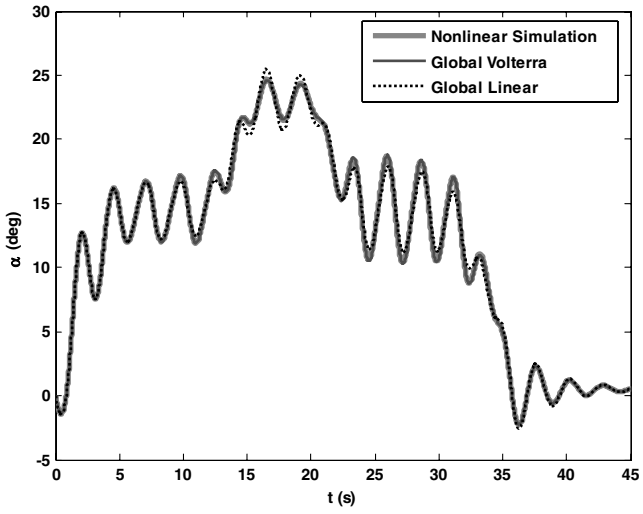

Fig. 11 Stair response test case.

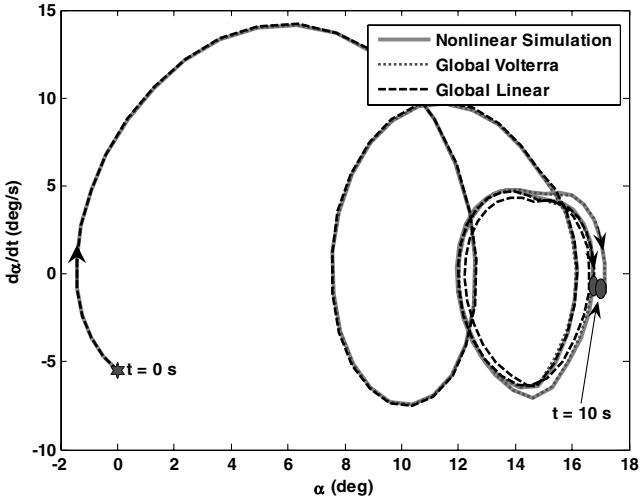

Fig. 12 Phase plane from $t = 0$ s to $t = 10$ s for stair response test case.

$$\begin{bmatrix}\dot{\alpha}\\ \dot{q}\end{bmatrix}=\begin{bmatrix}-0.153 & 1\\ -5.73 & 0\end{bmatrix}\begin{bmatrix}\alpha\\ q\end{bmatrix}+\begin{bmatrix}-1.834\\ 8.595\end{bmatrix}\delta_e+\begin{bmatrix}8.715\\ 2.865\end{bmatrix}$$
$$18.87\ \text{deg} < \alpha \le 28\ \text{deg} \tag{19d}$$

The piecewise global Volterra approach and its accuracy are evaluated by three test cases with different input waveforms. The first input signal is assigned to primarily validate the submodels and the local behavior around certain operating conditions. The input is designed to have a fast, smooth change from 0 to −9.5 deg within 5 s. The input is then held at −9.5 deg, as shown in Fig. 4. The final value is selected to lie inside a nonlinear region (prestall/stall). During the first 5 s, there is no large difference between the linear model and the Volterra model as shown in Fig. 5. When the input starts to settle at $\delta_e = -9.5$ deg, the nonlinearity becomes dominant and its signature appears in the system behavior as a limit cycle waveform. In this period of time, the linear model shows a significant inability to capture this phenomenon. The linear model responds as an oscillatory damped system, because this model has no mechanism to generate such a phenomenon. On the other hand, the Volterra model shows more adequacy to render the system behavior through the second-order kernel h_2. The maximum amplitude error from the Volterra model for this approximately 4.5-deg-amplitude angle-of-attack limit cycle is 0.5 deg compared with 4.5 deg error in the linear model case. Both models do a good job of predicting the oscillation frequency. Based on this test case, the Volterra model shows ample

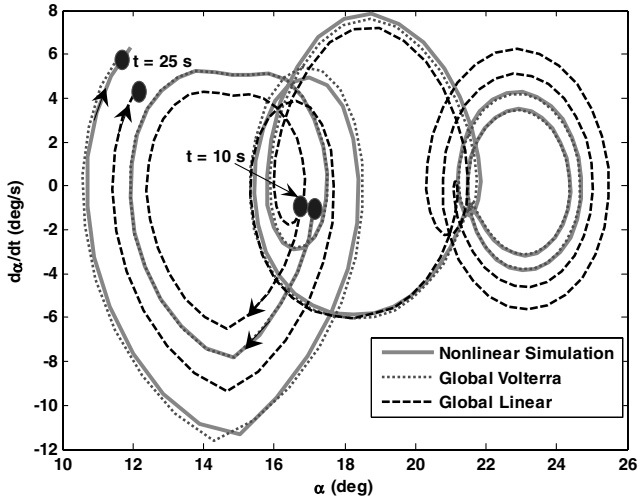

Fig. 13 Phase plane from $t = 10$ s to $t = 25$ s for stair response test case.

ability to capture nonlinear behavior with reasonable qualitative and quantitative accuracy in the submodels (see Fig. 5).

In addition to the time response, a parametric time track is visualized over the phase plane for more analysis as shown in Fig. 6, where the rate of attack angle is plotted against the attack angle from $t = 0$ s to $t = 100$ s. During the first 5 s, there is no difference between the linear model track and the Volterra model track compared with the nonlinear simulation track. As the tracks start to intersect the vertical line of $\alpha = 14.7$ deg (minimum value of C_z, see Fig. 1), each track heads in a different way. The linear model track forms a spiral orbit converging at the attractor point ($\alpha = 14.7$ deg and $d\alpha/dt = 0$). This track is a damped oscillatory response. In contrast, the Volterra model and nonlinear simulation tracks head away to form a limit cycle with a semicardioid shape. To the left side of the line $\alpha = 14.7$ deg, the cardioid path has a tendency to move towards the attractor point or a tendency for stability (negative slope of C_z). After the track crosses to the right of this line, the tendency is inverted to instability or divergence (positive slope of C_z). Hence, the indentation near $\alpha = 14.7$ deg and $d\alpha/dt > 0$ appears when moving from a stable C_Z to an unstable C_Z, and likewise the protuberance near $\alpha = 14.7$ deg and $d\alpha/dt < 0$ appears when moving from an unstable C_Z to a stable C_Z. Eventually a balance between these two competing effects ensues and the system forms a limit cycle with smooth curvature around the line $\alpha = 14.7$ deg. Note the linear model track crosses this line with a slope discontinuity. Observations based on the phase plane (see Fig. 6) imply the Volterra model has high capability to render smooth inverting of the slope of C_Z from negative to positive values in the same way as the nonlinear simulation, which the linear model cannot provide.

The second input is assigned to have more excitation range and to move over and return across the subregions in rapid succession. The input starts to excite the dynamic behavior from the prestall linear region going through the entire space (from $\delta_e = 0$ deg to $\delta_e = -14$ deg), returning back to the prestall linear region ($\delta_e = -5$ deg), and finally settling in the prestall/stall nonlinear region as shown in Fig. 7. Although both linear and Volterra models have a close qualitative behavior in rendering system dynamics during the first 50 s, the linear system proves very poor in rendering system behavior in the final duration (from $t = 50$ s to $t = 120$ s). This observation from the second test case (see Fig. 8) indicates that linear and Volterra models have the same level of accuracy if switching between regions is very fast (sharp change in input). The breakdown of the linear model beyond $t = 50$ s is again due to an inability to perform sustained oscillation. The Volterra model again has less than 0.5 deg error in angle of attack across the entire test case relative to the nonlinear simulation. Also, the phase plane shown in Fig. 9 leads to the same conclusion from the time response. Thus the linear model and Volterra model tracks have the same performance during the fast change in the input. However the linear track loses its accuracy when the input is held at the prestall/stall nonlinear region.

Because of the insensitivity to rapid input changes, test case 3 assigns an input with smooth movement over the entire space as shown in Fig. 10. This input tries to imitate the real movement of input experienced in practice (generated from biopilot or autopilot), which should be dynamically smooth. Figure 11 shows that linear and Volterra models are quantitatively close. The maximum error developed by the linear model is 1.2 deg compared with 0.4 deg developed by the Volterra model for an overall 25 deg change in angle of attack. From the qualitative perspective, the Volterra model is more adequate (see Fig. 11), especially in rendering system hysteresis. In the first duration (from $t = 0$ s to $t = 15$ s), both linear and Volterra models provide close results. Conversely, the linear model starts to have less accuracy in the second half of the maneuver (from $t = 20$ s to $t = 40$ s). Thus, some residual state is accumulated in the system memory when passing through the nonlinear region in the first duration. This accumulated memory appears in the second half of the maneuver, primarily as amplitude growth. Such a phenomenon cannot be captured by the linear model as the Volterra model does. After the memory effect dissipates both systems return to the same equilibrium at $t = 45$ s.

Because of the large excitation in this test case, a phase plane is plotted in two segments. Figure 12 shows the phase plane in the first 10 s for when the system crosses from the linear region to the nonlinear regions. As it appears in Fig. 12, both linear and Volterra model tracks follow the nonlinear simulation. However, the linear model track starts to deviate as the system enters the nonlinear region. Figure 13 shows the second window of the phase plane from $t = 10$ s to $t = 25$ s. The three tracks rotate around the point defined by $\alpha = 14.7$ deg and $d\alpha/dt = 0$ deg/s by cardioid orbits (prestall/stall region). The input then moves the track to rotate in another circular orbit (stall/poststall region) around the point defined by $\alpha = 23$ deg and $d\alpha/dt = 0$ deg/s. Although linear and Volterra model tracks have the same shape, the Volterra model shows a superior performance with higher accuracy than the linear model. The linear track is incapable of producing the radius of this circular orbit in the nonlinear system. All these test cases validate the capability of the Volterra model to be quite adequate in rendering the global behavior of the system with nonlinear phenomena (limit cycle and amplitude hysteresis memory effect).

The cost of computing the Volterra-kernel-based responses compared with the nonlinear and linear simulations using a modern desktop computer is listed in Table 3. Run time for the Volterra simulation is comparable to but less than the nonlinear simulation time and always greater than the time for linear simulation. This result emphasizes one merit of using the proposed piecewise global Volterra approach. If a traditional Volterra approach was used, a polynomial of ninth-order is required to fit the relation between C_z and α. Approximately nine kernels would be required to capture the system behavior or 18 states would be required in the pseudostate space model. Instead, the piecewise global approach replaces this model by four submodels with two kernels or four states, each of which is computationally more efficient.

Analysis of flight vehicle dynamic behavior, based on the Volterra model kernels, is addressed next. Although a differential form of Volterra theory using piecewise interpolation was implemented for simulation accuracy purposes, the integral form can also be used in creating the global model. The primary intent here is dynamic analysis based on the analytical kernel framework. To that effect, the submodels of local Volterra series are employed in a lookup table procedure using linear interpolation. In this way a new dimension is added to the series kernels. For example, the first input kernel will have two arguments $h_1(t_1, \delta_{eo})$ instead of one $h_1(t_1)$ where δ_{eo} is the operating point around which the submodel is constructed. Figures 14 and 15 show the global Volterra kernels for zero and first orders. These kernels appear as surfaces across the two independent variables. The values of the zero-order kernel $h_0(t_1, \delta_{eo})$ and the first-order kernel $h_1(t_1, \delta_{eo})$ are nonzero across all subspaces. On the other hand, the second kernel $h_2(t_1, t_2, \delta_{eo})$ is nonzero in three regions (prestall/stall, stall/poststall, and poststall), and has a zero value elsewhere. The hypersurface representing the second kernel cannot be fully plotted in three dimensions. For visualization, Fig. 16 shows the second kernel hypersubsurface for the prestall/stall region.

The surface shown in Fig. 14 reflects how the zero kernel's nature changes temporally and from one flight regime to another. This surface primarily represents the initial condition response. First note that for all elevator values, the kernel, with respect to time, starts at

Table 3 Computational cost of each simulation technique

Test case	Linear simulation time, s	Nonlinear simulation time, s	Volterra simulation time, s
Step	0.092	0.124	0.109
Bang-bang	0.108	0.141	0.122
Stair	0.125	0.156	0.138

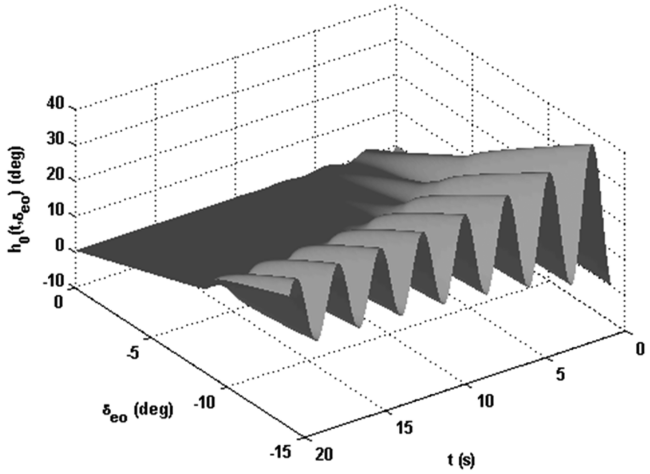

Fig. 14 Global zero-order Volterra kernel.

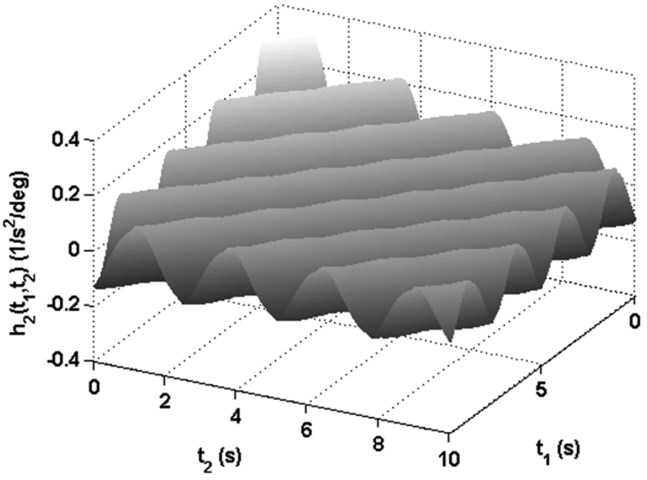

Fig. 16 Second-order Volterra kernel in prestall/stall subspace.

zero. This initial value is consistent with how the kernels were computed for $\alpha = 0$ deg initially. At a low value of δ_{eo}, $h_0(t_1, \delta_{eo})$ has a linear characteristic waveform with respect to the time axis. The waveform of $h_0(t_1, \delta_{\text{eo}})$ looks like an underdamped second-order system. As time increases the amplitude of the conducted oscillation decreases and tends to zero, leaving a nonzero steady-state value. The frequency and damping values from this region are consistent with those from Eq. (19a). Conversely, at a high value of δ_{eo}, the nonlinearity becomes important, and $h_0(t_1, \delta_{\text{eo}})$ exhibits a nonlinear or nonexponential shaped waveform. The nonlinearity appears here as a self starting or initial condition excited limit cycle within $h_0(t_1, \delta_{\text{eo}})$. As time increases, the amplitude of this oscillation is constant at an approximate value of 9.5 deg, whereas the corresponding frequency is 2.4 rad/s. In between the δ_{eo} extremes, $h_0(t_1, \delta_{\text{eo}})$ gradually changes from a linear to a nonlinear waveform proportional to elevator setting.

The waveform of $h_1(t_1, \delta_{\text{eo}})$ can be fairly well modeled as an underdamped second-order system over the entire space in the sense that $h_1(t_1, \delta_{\text{eo}})$ represents the linear portion of the system. The characteristic of this linear waveform changes from one subspace to another. Figure 15 shows how the characteristics of the plunging force coefficient C_Z have been projected onto the $h_1(t_1, \delta_{\text{eo}})$ waveform. The observation indicates a higher damped oscillatory response (relatively high negative slope of C_Z) in the prestall subspace, and a lower damped oscillatory response in the poststall subspace (relatively low negative slope of C_Z). In the poststall region, the oscillation amplitude continues to decrease for large time but at a rather slow rate. The frequency and damping values for the two regions in Fig. 15 roughly correspond to values extracted from the linear model in Eqs. (19a–19d). In between the two distinct regions in Fig. 15, a sharp change is observed in the two stall subspaces. This sharp change is expected, because the difference between the operated elevator deflection in the prestall/stall subspace ($\delta_{\text{eo}} = -9.5$ deg) and stall/poststall subspace ($\delta_{\text{eo}} = -11$ deg) is only 1.5 deg. This difference means that any small change in δ_e leads to a significant change in system behavior or a sharp change in $h_1(t_1, \delta_{\text{eo}})$.

Figure 16 shows the second kernel in the prestall/stall subspace. This kernel represents the source of input excited limit cycle behavior. Thus, the waveform of this kernel reflects a sustained constant amplitude oscillation. Note the frequency of oscillation in Fig. 16, when moving along the diagonal, is 4.4 rad/s, approximately twice that in Fig. 14 for high δ_{eo} values. However, when moving along only one of the time axes, the frequency is 2.2 rad/s, consistent with Fig. 14 and observed oscillations in all three test case responses. Based on all these observations, it can be indicated that the h_0 kernel represents one of the nonlinearity's signatures imbedded in the system's memory (homogenous induced limit cycle), the h_1 kernel represents a linear behavior (damped oscillatory response) of the system with an arbitrary input, and the h_2 kernel is the nonlinear behavior of the system with the input history (nonhomogenous induced limit cycle). Building such global kernels provides a tool to predict and evaluate the system behavior from one flight region to another before exercising the nonlinear simulation tool.

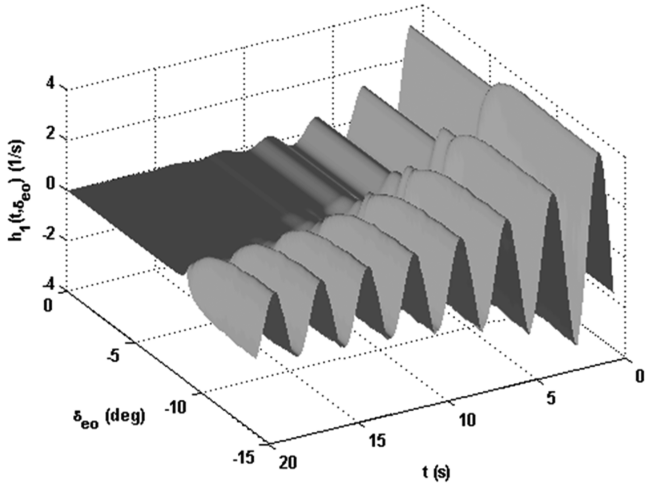

Fig. 15 Global first-order Volterra kernel.

VII. Conclusions

In this work, the development of a nonlinear global dynamic analysis modeling procedure based on piecewise Volterra kernels is studied. The procedure opens a new window for practical use of Volterra theory when applied to systems with a strong overall nonlinearity requiring several high-order kernels by decomposing the nonlinearity into weaker component nonlinearities appearing in several operational subregions requiring fewer kernels. The technique was usefully applied to an approximate low-order nonlinear pitch–plunge model. The piecewise interpolated Volterra kernels yielded sufficient accuracy for analysis of dynamic characteristics associated with high attack angle stall and lift recovery nonlinearity. The underlying functional framework of Volterra theory was used to trace the aerodynamic nonlinearity through the vehicle dynamics (state-dependent kernel and the first- and second-order input-dependent kernels) to resulting response behavior such as limit cycling amplitude and frequency, as well as transient oscillation frequency and decay rate, across a broad region of operating conditions. This information is unobtainable from the linear piecewise molding approach and would be difficult to obtain from pure nonlinear simulation. The new modeling procedure offers information beyond that available from standard linear and nonlinear techniques. Results from this application appear promising and warrant further study for more complex nonlinear systems.

References

[1] Volterra, V., *Theory of Functionals and of Integral and Integro-Differential Equations*, Dover, New York, 1958.

[2] Rugh, J. W., *Nonlinear System Theory: The Volterra/Wiener Approach*, John Hopkins Univ. Press, Baltimore, MD, 1981, pp. 37–41.

[3] Wiener, N., "Response of a Nonlinear Device Noise," Massachusetts Institute of Technology Radiation Laboratory Rept. 165, Cambridge, MA, 1942.

[4] Brilliant, M., "Theory of the Analysis of Nonlinear Systems," Massachusetts Institute of Technology Radiation Laboratory, Rept. 345, Cambridge, MA, 1958.

[5] George, D., "Continuous Nonlinear Systems," MIT RLE, Rept. 355, 1959.

[6] Brus, L., "Nonlinear Identification of an Anaerobic Digestion Process," *Proceedings of 2005 IEEE Conference on Control Application*, IEEE Publications, Piscataway, NJ, Aug. 2005, pp. 137–142.

[7] Gray, W. S., and Nabet, B., "Volterra Series Analysis and Synthesis of a Neural Network for Velocity Estimation," *IEEE Transactions on Systems, Man, and Cybernetics*, Vol. 29, No. 2, April 1999, pp. 190–197.
doi:10.1109/3477.752793

[8] Duffy, P. K., "Nonlinear Green's Function Method for Transonic Potential Flow," Ph.D. Dissertation, Department of Mechanical and Aerospace Engineering, Case Western Reserve University, Cleveland, OH, 1986.

[9] Silva, W. A., "Reduced-Order Models Based on Linear and Nonlinear Aerodynamic Impulse Responses," *Proceedings of AIAA 40th Structures, Structural Dynamics, and Materials Conference*, AIAA, Reston, VA, April 1999, pp. 638–648.

[10] Silva, W., "A Methodology for Using Nonlinear Aerodynamics in Aeroservoelastic Analysis and Design," *Proceedings of AIAA 32nd AIAA/ASME/ASCE/AHS/ASC Structures, Structural Dynamics, and Materials Conference*, AIAA, Reston, VA, April 1991, pp. 1951–1963.

[11] Silva, W., "Application of Nonlinear Systems Theory to Transonic Unsteady Aerodynamic Responses," *Journal of Aircraft*, Vol. 30, No. 5, Oct. 1993, pp. 660–668.
doi:10.2514/3.46395

[12] Marzocca, P., Silva, W., and Librescu, L., "Open/Closed-Loop Nonlinear Aeroelasticity for Airfoils via Volterra Series Approach," *Proceedings of AIAA 43rd AIAA/ASME/ASCE/AHS/ASC Structures, Structural Dynamics, and Materials Conference*, AIAA, Reston, VA, April 2002.

[13] Marzocca, P., Silva, P., and Librescu, L., "Nonlinear Open-/Closed-Loop Aeroelastic Analysis of Airfoils via Volterra Series," *AIAA Journal*, Vol. 42, No. 4, April 2004, pp. 673–686.
doi:10.2514/1.9552

[14] Marzocca, P., Lazzaro, R., and Librescu, L., "Flutter/Aeroelastic Response of Panels via a Combined Galerkin-Volterra Series Approach," *Proceedings of AIAA 45th AIAA/ASME/ASCE/AHS/ASC Structures, Structural Dynamics, and Materials Conference*, AIAA, Reston, VA, April 2004.

[15] Marzocca, P., Librescu, L., and Silva, W., "Volterra Series Approach for Nonlinear Aeroelastic Response of 2-D Lifting Surfaces," *Proceedings of AIAA 42nd AIAA/ASME/ASCE/AHS/ASC Structures, Structural Dynamics, and Materials Conference*, AIAA, Reston, VA, April 2001.

[16] Baldelli, H. D., Lind, R., and Brenner, M., "Nonlinear Aeroelastic/Aeroservoelastic Modeling by Block-Oriented Identification," *Journal of Guidance, Control, and Dynamics*, Vol. 28, No. 5, Oct. 2005, pp. 1056–1064.
doi:10.2514/1.11792

[17] Brenner, J. M., and Richard, J. P., "Aeroservoelastic Model Validation and Test Data Analysis of the F/A-18 Active Aeroelastic Wing," NASA TM-2003-212021, 2003.

[18] Silva, W., "Simultaneous Excitation of Multiple-Input/Multiple-Output CFD-Based Unsteady Aerodynamic Systems," *Journal of Aircraft*, Vol. 45, No. 4, July–Aug. 2008, pp. 1267–1274.
doi:10.2514/1.34328

[19] Mohler, R. R., "Nonlinear Stability and Control Study of Highly Maneuverable High Performance Aircraft," NASA OSU-ECE Rept. 91-01, 1991.

[20] Stalford, H., Baumann, W. T., Garrett, F. E., and Herman, T. L., "Accurate Modeling of Nonlinear System Using Volterra Series Submodels," *Proceedings of the 6th American Control Conference*, Vol. 2, July 1987, pp. 886–891.

[21] Suchomel, C. F., "Nonlinear Flying Qualities—One Approach," *Proceedings of AIAA 25th Aerospace Sciences Meeting*, AIAA, New York, Jan. 1987, pp. 1–10.

[22] Omran, A., and Newman, B., "Global Aircraft Dynamics Using Piecewise Volterra Kernels," *Proceedings of AIAA Atmospheric Flight Mechanics Conference*, AIAA, Reston, VA, Aug. 2008.

[23] Marmarelis, Z. V., *Nonlinear Dynamic Modeling of Physiological Systems*, Wiley, New York, 2004, pp. 29–142.

[24] Zhang, H., Zhang, C., Chen, Z., and Xiang, W., "OFS Model-Based Adaptive Control for Block-Oriented Non-Linear Systems," *Transactions of the Institute of Measurement and Control (London)*, Vol. 28, No. 3, May 2006, pp. 206–118.

[25] Franz, M., and Scholkopf, B., "A Unifying View of Wiener and Volterra Theory and Polynomial Kernel Regression," *Neural Computation*, Vol. 18, No. 12, Dec. 2006, pp. 3097–3118.
doi:10.1162/neco.2006.18.12.3097

[26] Soni, A., "Control-Relevant System Identification Using Nonlinear Volterra and Volterra Laguerre Models," Ph.D. Dissertation, School of Engineering, Univ. of Pittsburgh, Pittsburgh, PA, 2006.

[27] Asyali, M., and Juusola, M., "Use of Meixner Functions in Estimation of Volterra Kernels of Nonlinear Systems with Delay," *IEEE Transactions on Bio-Medical Engineering*, Vol. 52, No. 2, Feb. 2005, pp. 229–237.
doi:10.1109/TBME.2004.840187

[28] Eskinat, E., Johanson, S., and Luben, W., "Use of Hammerstein Models in Identification of Nonlinear Systems," *AIChE Journal*, Vol. 37, No. 2, Feb. 1991, pp. 255–268.
doi:10.1002/aic.690370211

[29] Narendra, K., and Gallman, P., "An Iterative Method for the Identification of Nonlinear Systems Using a Hammerstein Model," *IEEE Transactions on Automatic Control*, Vol. 11, No. 3, 1966, pp. 546–550.
doi:10.1109/TAC.1966.1098387